Development of an Organic Acid-Based Process for Rare Earth Recovery from NdFeB Magnets

Downloaded from: https://research.chalmers.se, 2026-11-11 12:07 UTC

Citation for the original published paper (version of record):

Petraglia, F., Garjulli, F., Rouquette, L. et al (2026). Development of an Organic Acid-Based Process for Rare Earth Recovery from NdFeB Magnets. Journal of Sustainable Metallurgy, In Press. http://dx.doi.org/10.1007/s40831-026-01659-w

N.B. When citing this work, cite the original published paper.

research.chalmers.se offers the possibility of retrieving research publications produced at Chalmers University of Technology. It covers all kind of research output: articles, dissertations, conference papers, reports etc. since 2004. research.chalmers.se is administrated and maintained by Chalmers Library

(article starts on next page)

Journal of Sustainable Metallurgy
https://doi.org/10.1007/s40831-026-01659-w

RESEARCH ARTICLE

Development of an Organic Acid-Based Process for Rare Earth Recovery from NdFeB Magnets

Fernanda Fajardo Nacif Petraglia[1] · Franco Garjulli[1] · Léa Marie Jacqueline Rouquette[2] · Martina Petranikova[2] · Jorge Alberto Soares Tenório[1] · Denise Crocce Romano Espinosa[1]

Received: 16 February 2026 / Accepted: 15 August 2026
© The Author(s) 2026

Abstract

The recovery of rare earth elements (REEs) from NdFeB magnets is essential for securing sustainable supply chains for critical materials. In this study, the leaching behavior of Nd, Pr, and Dy was comparatively evaluated using five organic acids (citric, malic, tartaric, oxalic, and acetic acids) under identical experimental conditions. Citric acid demonstrated the highest leaching efficiency and was selected for further process optimization. A design of experiments (DoE) approach was applied to assess the combined effects of solid-to-liquid ratio, temperature, and time at a fixed citric acid concentration of 1.5 mol L^{-1}, revealing a multidimensional operational window capable of achieving high REE solubilization rather than a single optimum condition. Two purification strategies were subsequently investigated: solvent extraction using di(2-ethylhexyl) phosphoric acid (D2EHPA), yielding a 99.3% pure REE product, and an oxidative precipitation route based on in situ oxalic acid formation, achieving 95.7% purity with reduced process complexity.

Graphical Abstract

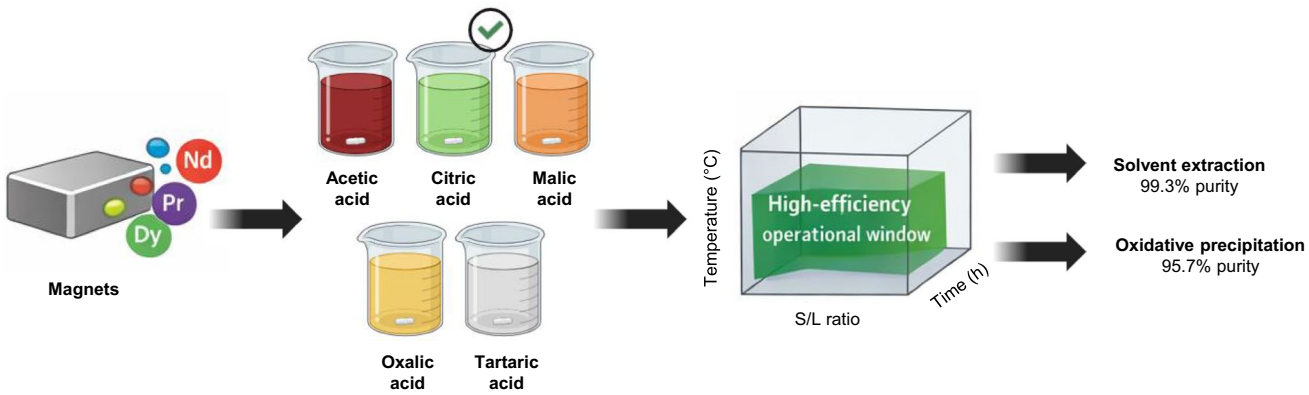

Keywords Recycling · Critical materials · Organic acids · Hydrometallurgy

The contributing editor for this article was Sadia Ilyas.

✉ Fernanda Fajardo Nacif Petraglia
fernandafajardo@usp.br

[1] Department of Chemical Engineering, Polytechnic School of the University of São Paulo (USP), Lago St., N° 250, São Paulo, SP 05508-080, Brazil

[2] Department of Chemistry and Chemical Engineering, Industrial Materials Recycling and Nuclear Chemistry, Chalmers University of Technology, Kemivägen 4, 41296 Gothenburg, Sweden

Introduction

The global transition toward a low-carbon economy rests on a persistent contradiction. Specifically, the recovery of rare earth elements (REEs), which are essential for electric mobility and wind energy generation, still relies predominantly on hydrometallurgical routes based on mineral acids [1]. Although effective, these reagents produce hazardous waste and require high chemical consumption. This results

Published online: 18 September 2026

in environmental impacts that contradict the eco-friendly principles expected from green technologies [2]. In addition, the primary supply of REEs is geographically concentrated, posing risks to global supply security [3] and often linked to considerable environmental burden, including radioactive waste generation and high water consumption [4].

In this context, recycling is no longer merely an environmentally favorable option but has become a strategic necessity. Urban mining offers a secondary source of REEs with concentrations significantly higher than those found in primary ores [5, 6]. Unlike conventional mining, where metals are dispersed within mineral matrices, electronic waste can present concentrations up to ten times higher [7, 8]. Among these residues, NdFeB magnets stand out due to their high content of Nd, Pr, and Dy embedded in a well-defined metallic structure, which facilitates their recovery through hydrometallurgical routes [9, 10].

Despite the high extraction efficiencies achieved with mineral acids such as H_2SO_4, HNO_3, and HCl, the high reactivity and limited selectivity of these agents compromise the overall sustainability balance of the process [1, 11]. In this scenario, organic acids have emerged as potential alternatives, operating through dissociation and complexation mechanisms that may enable a more controlled leaching of REEs [12, 13]. Compounds such as citric [10], malic [12], tartaric [14], oxalic [15], and acetic [16] acids have been individually investigated, demonstrating promising results under various experimental conditions. However, comparative assessments of different organic acids under equivalent operational parameters remain limited, making direct comparison of their performance and selection of the most suitable lixiviant challenging.

To address this knowledge gap, the present work aimed to develop and optimize a hydrometallurgical route for REE recovery from NdFeB permanent magnets through the comparative evaluation of five organic acids (citric, malic, tartaric, oxalic, and acetic acids). Initially, a systematic benchmarking study was conducted under identical experimental conditions to identify the most promising lixiviant. Subsequently, a design of experiments (DoE) approach was applied to evaluate and optimize the combined effects of acid concentration, solid-to-liquid ratio, temperature, and leaching time. Finally, a downstream purification step was investigated to obtain a high-purity REE concentrate, consolidating an integrated organic-acid-based recovery route.

Materials and Methods

Sample Preparation

NdFeB magnets obtained from a Danish company, with dimensions of 2.0 × 2.0 mm, were used in this study. These magnets were not recovered from end-of-life products or industrial waste but were selected because their chemical composition is representative of NdFeB magnets commonly found in hard disk drives. The magnets were processed at the Industrial Material Recycling Group at Chalmers University of Technology (Sweden). The samples were thermally demagnetized at 400 °C for 60 min in a muffle furnace (Entech, Sweden), then comminuted using a Vibratory Disc Mill RS 200 (Retsch) at 720 rpm for 90 s, and finally sieved to a particle size of < 500 µm.

Characterization

The chemical composition of the magnets was determined in triplicate by digesting the samples in aqua regia (HCl/HNO_3, 3:1 v/v – HCl: 37% w/w, Merck Millipore; HNO_3: 69% w/w, Suprapur, Merck), at 22 ± 1 °C for 60 min to determine the chemical composition. The solutions obtained were filtered, diluted in HNO_3 3%, and analyzed by inductively coupled plasma optical emission spectroscopy (ICP-OES). The crystalline phases of the material were obtained using X-ray diffraction (XRD, D8 Discover, Bruker) with Cu Kα radiation (λ = 1.5418 Å) operating at 30 kV and 10 mA, 2θ° sweep from 20° to 80°, variation of 0.02° and speed of 2° min^{-1}.

Evaluation of Leaching Agents

Acetic acid, citric acid, malic acid, oxalic acid, and tartaric acid were evaluated as leaching agents. The experiments were carried out in 100 mL glass beakers at 22 ± 1 °C under agitation (360 rpm). A total of 1.0 g of material was used in each experiment, and the solid-to-liquid (S/L) ratio was fixed at 1/30 g mL^{-1} [10]. Leaching was carried out at 2 h and 24 h, varying the acid concentrations according to their solubility limit [12, 17]. The leaching efficiency was calculated according to Eq. 1, where $[M]$ is the concentration of the element in the liquor (mg L^{-1}), V_l is the final volume (L), $[E]$ is the concentration of the element in the material (wt%), and w_0 is the initial sample (mg).

$$L(\%) = \frac{[M].V_l}{[E].w_0}. \quad (1)$$

Design of Experiments

After identifying the acid with the best performance—citric acid—the leaching was optimized through a DoE approach using response surface methodology (RSM) to evaluate the effects of key variables. A faced-centered composite design (FCC) was used with three factors: leaching time (x_1), S/L ratio (x_2), and leaching temperature (x_3). Their coded levels are presented in Table 1, where (−1) represents the lowest

Table 1 Coded levels of the independent variables (time, S/L ratio, and temperature)

Factor		Level		
		−1	0	+1
x_1	Time (h)	1	2	3
x_2	S/L ratio	1/10	1/15	1/20
x_3	Temperature (°C)	25	50	75

value and (+1) the highest. A total of eighteen experiments (Appendix Table 8) were carried out in random order to minimize systematic errors and better simulate real conditions. The central point (0, 0, 0) was replicated four times (experiments 9–12) to estimate the experimental error. The acid concentration was fixed at 1.5 mol L^{-1}. Based on experimental responses (leaching yield of each element), regression equations were constructed to model the process and to map the responses as a function of the independent variables within the investigated range, using the regression analysis tool in Microsoft Excel.

REE Separation

Solvent extraction (SX) and precipitation experiments were performed for the purification of REEs. The initial pH of the aqueous phase was adjusted to 3.1 ± 0.1 using 2.0 mol L^{-1} H_2SO_4 or 5.0 mol L^{-1} NaOH and measured with a Radiometer Analytical MeterLab pH meter. All experiments were carried out in triplicate.

Solvent Extraction

SX was evaluated for the separation of REEs. Di(2-ethylhexyl)phosphoric acid (D2EHPA; 97%, Sigma-Aldrich) was selected for the SX experiments because it is one of the most widely applied extractants for REEs in the literature [18, 19]. The aqueous phases were prepared by diluting the extractant in Isopar-L (97%, Sigma-Aldrich) and tributyl phosphate (TBP, 3%, ExxonMobil). The extractant concentration (0.1–0.5 mol L^{-1}), aqueous-to-organic phase ratio (A/O) (1.0–2.5), and contact time (5–30 min) were evaluated.

The experiments were performed in a 3.5 mL glass vial by combining equal volumes (1 mL) of the organic and aqueous phases. The mixtures were shaken (Vibrax® VXR Basic, IKA) at 1500 rpm and 22 °C ± 1 °C. After mixing, the vials were centrifuged for 5 min (5000 rpm, Ohaus Frontier™ 5000 Series Multi Pro). The aqueous phases were collected, diluted in 3% HNO_3, and analyzed by ICP-OES.

Extraction efficiency and metal selectivity were quantified through the distribution ratio (D_i) and the separation factor (SF). The coefficient D_i was calculated according to Eq. 2, using the equilibrium metal concentrations in the organic ($[M_i]_{org}$) and aqueous ($[M_i]_{aq}$) phases. The separation factor (Eq. 3) was used to evaluate the selectivity of extraction of REEs relative to Fe, where D_i and D_j represent the distribution ratios of metals i and j, respectively (Fe as j).

$$D_i = \left(\frac{[M_i]_{org}}{[M_i]_{aq}} \right), \tag{2}$$

$$SF_{\frac{i}{j}} = \frac{D_i}{D_j}. \tag{3}$$

The stripping behavior of REEs was investigated using HCl as stripping agent, at concentrations ranging from 0.1 to 0.7 mol L^{-1}. The experiments were conducted following the same procedure described for the SX tests. In this case, the aqueous phase consisted of freshly prepared acid solutions, while the organic phase corresponded to the REE-loaded extract obtained from the SX stage. The stripping efficiency for each element was determined based on Eq. 4, using the concentration of metal in the aqueous phase after stripping (C_i) and the initial concentration in the loaded organic phase.

$$Stripping(\%) = 100\left(\frac{C_o - C_i}{C_o} \right). \tag{4}$$

Precipitation

As an alternative, precipitation experiments were performed in 50 mL beakers under agitation (200 rpm) at 22 °C ± 1 °C for 10 min. H_2O_2 (PA grade, 52% w/w) was added at a liquid-to-liquid ratio of 1/10 to oxidize Fe^{2+} to Fe^{3+} and promote its selective precipitation. After the reaction time, the suspensions were filtered (55 mm Ø, qualitative filter paper, Circles, Whatman™). The filtrates were collected, diluted in 3% HNO_3, and analyzed by ICP-OES. The powders were analyzed by XRD to identify their crystalline phases. The precipitation efficiency for each metal was calculated using Eq. 5, where C_o and C_i represent the initial and final concentrations of the metal in solution, respectively.

$$Precipitation(\%) = \frac{C_o - C_i}{C_o}.100. \tag{5}$$

Results and Discussion

Characterization

The elemental characterization of the magnets is presented in Table 2. The magnets were mainly composed of Fe (57.7% ± 1.0), Nd (20.5% ± 0.5), and Pr (7.0% ± 0.4), as well as

Table 2 Elemental composition of the magnet powder

Element	Nd	Fe	B	Pr	Dy	Co	Cu	Ni
wt (%)	20.5±0.5	57.7±1.0	1.8±0.1	7.0±0.4	0.3±0.1	0.9±0.1	0.7±0.1	1.1±0.1

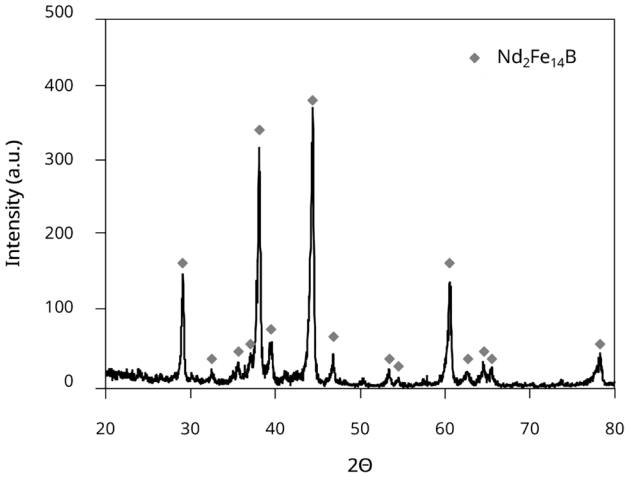

Fig. 1 REE magnet X-ray diffraction pattern after demagnetization

B, Dy, Co, and Cu. Ni, originating from the coating layer, was also quantified at around 1.1% wt [20]. Although the magnets were not obtained from waste electronic devices, their composition is comparable to that of magnets typically used in hard disk drives [21], supporting the applicability of the proposed process to the recycling of such devices. The X-ray diffraction patterns of the magnets (Fig. 1) show characteristic phases of $Nd_2Fe_{14}B$ [9], corroborating the chemical characterization.

REE Leaching

Choosing the Organic Acid

Leaching experiments were carried out using acetic acid, citric acid, malic acid, oxalic acid, and tartaric acid as leaching agents. The time and concentration of the acid were evaluated while the S/L ratio was fixed at 1/30 at 22 ± 1 °C. Leaching efficiency of REE for (a) 2 h and (b) 24 h can be seen in Fig. 2.

The variation in acid concentration had no influence on the leaching of REEs, regardless of reaction time, for any of the leaching agents studied except for tartaric acid. However, by increasing the reaction time from 2 to 24 h, REE leaching using acetic, citric, and malic acid achieved approximately 100% recovery at all concentrations. Tartaric acid changed its behavior after 24 h of leaching (Fig. 2b). At 0.25 mol L^{-1} tartaric acid, 17.6% REE were leached; however, increasing the concentration to 1.0 mol L^{-1} reduced REE leaching to 1.6%. This behavior may be associated with the formation of poorly soluble REE-tartrate species at higher tartaric acid concentrations, as reported in previous studies [14].

The interaction between tartaric acid and REEs is related to the presence of carboxylate groups capable of coordinating metal ions. This interpretation is supported by Fourier transform infrared (FTIR) spectroscopy analysis of the leaching residue (Fig. 3), which showed bands associated with carboxylate groups (1577 and 1409 cm^{-1}) and REE-oxygen interactions (655 cm^{-1}), suggesting the presence of tartrate-related species in the solid phase. Tian et al. [22] studied REE leaching using HCl, evaluating selective leaching using tartaric acid as a complexing agent. At concentrations below 0.3 mol L^{-1}, complexes with Fe were observed, enabling selective REE leaching. By increasing the tartaric acid concentration, REE leaching decreased due to the formation of insoluble REE complexes. These findings indicate that tartaric acid may act not only as a leaching agent but also as a complexing agent, influencing REE solubility depending on its concentration.

After 24 h of reaction, no measurable concentration of REEs was detected in the leachate, regardless of oxalic acid concentration or reaction time. Oxalic acid was selected based on literature reporting its potential for selective Fe leaching [23–25]. The absence of solubilized REEs is likely related to the low solubility of REE oxalates [26, 27], which may promote precipitation under the experimental conditions, thereby limiting the concentration of REEs in solution. Furthermore, the formation of insoluble oxalate phases on the particle surface may have contributed to surface passivation, hindering further dissolution. Only about 1% of Fe was leached. Although acid availability at the applied S/L ratio (1/30) may also have influenced the extent of Fe solubilization, an estimated oxalic acid concentration of approximately 0.84 mol L^{-1} would be required to satisfy the stoichiometric demand, exceeding the concentrations investigated in this study.

Based on preliminary experiments, a correlation was observed between the time and the leaching rate. This observation is consistent with the findings reported by Niskanen et al. [28], who identified temperature/time and acid concentration/S/L ratio as compensatory variables in organic acid leaching systems. Such compensatory effects are closely related to the dissociation behavior of organic acids, which occurs gradually as ions become available for leaching, depending on their pKa values [13].

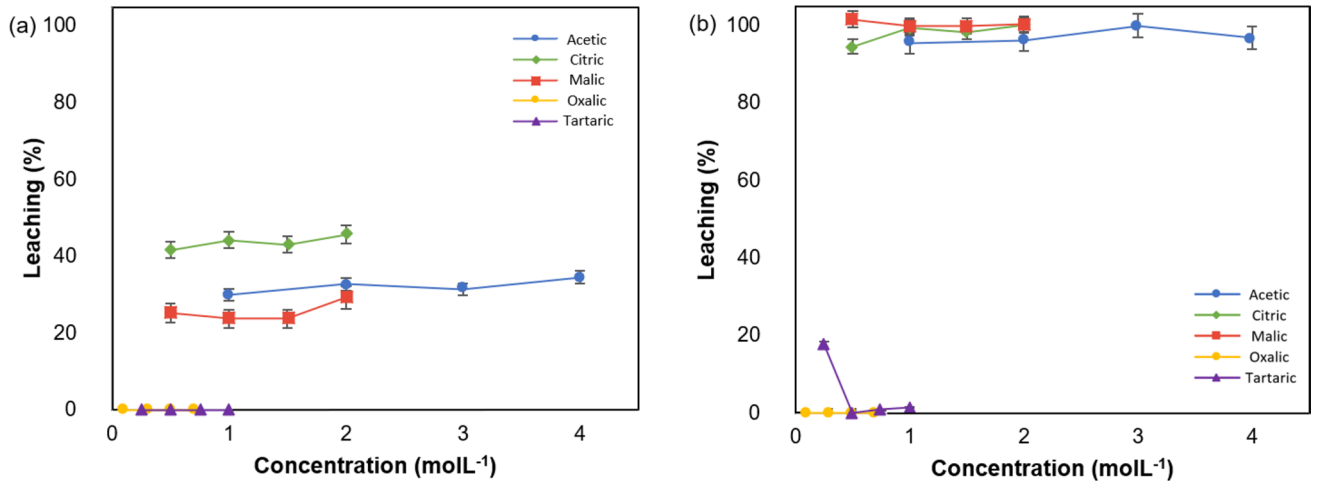

Fig. 2 Leaching of REE using organic acids as leaching agents for **a** 2 h and **b** 24 h (S/L ratio of 1/30 at 25 °C)

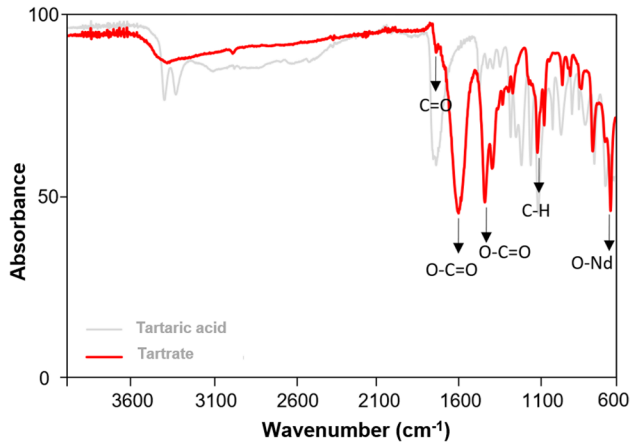

Fig. 3 FTIR spectrum of the leaching residue obtained after tartaric acid leaching of NdFeB magnets

In this comparative evaluation, acetic, citric, and malic acids showed the highest REE leaching efficiencies under the investigated conditions, in agreement with previous studies [12, 29–32]. Seeking a viable and stable process, acetic acid was discarded due to post-leaching precipitation, with approximately 10% of REEs and Fe observed in the filtrate 24 h after the experiments. Among the remaining acids, citric acid exhibited the lowest standard deviation among triplicates (< 2%), indicating higher reproducibility and greater process stability under the evaluated conditions. Therefore, considering leaching efficiency, citric acid was selected as the most suitable lixiviant for subsequent optimization and purification studies.

The leaching reactions of REEs with citric acid are shown in Eqs. 6, 7, 8, 9, 10, 11, and 12. Citric acid undergoes successive deprotonation steps (Eqs. 6, 7, 8) [33], and according to the speciation diagram (Appendix Fig. 7), H_2Cit^- is the predominant species at the liquor pH (3.1). Initially, REEs are dissolved by proton attack, generating RE^{3+} ions in solution (Eq. 9). Due to the presence of citrate species, equilibrium complexation reactions may occur, resulting in the formation of soluble REE–citrate complexes (Eqs. 10, 11, 12). However, under the investigated pH conditions (3.1), the lower availability of the fully deprotonated citrate species (Cit^{3-}) limits complexation, and free REE ions coexist with partially complexed species in the leachate [12]. The complexation equations are presented as global equilibrium reactions and do not imply that Cit^{3-} is the predominant free citrate species at pH 3.1.

$$H_3Cit_{(aq)} + H_2O \rightleftharpoons H_2Cit^-_{(aq)} + H_3O^+_{(aq)}, \quad (6)$$

$$H_2Cit^-_{(aq)} + H_2O \rightleftharpoons HCit^{2-}_{(aq)} + H_3O^+_{(aq)}, \quad (7)$$

$$HCit^{2-}_{(aq)} + H_2O \rightleftharpoons Cit^{3-}_{(aq)} + H_3O^+_{(aq)}, \quad (8)$$

$$2RE^0_{(s)} + 6H_3O^+_{(aq)} \rightleftharpoons 2RE^{3+}_{(aq)} + 3H_{2(g)} + 6H_2O_{(l)}, \quad (9)$$

$$RE^{3+}_{(aq)} + Cit^{3-}_{(aq)} + H_3O^+_{(aq)} \rightleftharpoons REHCit^+_{(aq)}, \quad (10)$$

$$RE^{3+}_{(aq)} + 2Cit^{3-}_{(aq)} \rightleftharpoons RE(Cit)^{3-}_{2(aq)}, \quad (11)$$

$$RE^{3+}_{(aq)} + 2Cit^{3-}_{(aq)} + H_3O^+_{(aq)} \rightleftharpoons RE(Cit)^{2-}_{2(aq)}. \quad (12)$$

Table 3 Leaching response of elements for each experiment

EC	pH	Variables			Leaching (%)				
		Time (×1)	S/L ratio (×2)	Temperature (×3)	B	Dy	Fe	Nd	Pr
1	2.5	1	1/10	25	7.3	21.4	21.4	29.1	27.5
2	2.9	3	1/10	25	19.2	47.8	47.1	51.9	53.0
3	2.2	1	1/20	25	8.1	23.0	20.4	29.6	31.3
4	2.5	3	1/20	25	20.9	52.3	53.6	57.6	55.3
5	3.6	1	1/10	75	44.9	91.2	100.0	90.5	86.3
6	3.6	3	1/10	75	47.4	97.0	100.0	100.0	99.5
7	2.9	1	1/20	75	47.7	100.0	100.0	100.0	98.4
8	2.8	3	1/20	75	48.3	100.0	100.0	100.0	98.1
9	3.2	2	1/15	50	43.3	97.8	100.0	99.4	95.2
10	3.1	2	1/15	50	42.1	98.2	100.0	100.0	93.4
11	3.1	2	1/15	50	47.2	96.8	100.0	99.3	92.3
12	3.2	2	1/15	50	42.2	96.3	100.0	98.7	94.9
13	3.1	1	1/15	50	34.4	79.2	90.3	82.5	82.0
14	3.2	3	1/15	50	50.3	100.0	100.0	100.0	97.6
15	3.4	2	1/10	50	44.0	89.3	100.0	93.2	88.7
16	2.8	2	1/20	50	46.7	100.0	100.0	100.0	94.4
17	2.7	2	1/15	25	14.1	34.8	33.6	39.9	40.5
18	3.1	2	1/15	75	48.7	97.2	100.0	100.0	93.8

DoE Leaching

The leaching responses of REEs (Nd, Pr, and Dy), Fe, Co, and B obtained from the experimental design are summarized in Table 3. The REEs and Fe exhibited a variation in leaching efficiencies, ranging from 21.4% to complete leaching (100%). In contrast, B consistently presented the lowest leaching efficiency, varying only between 7.3% and 50.3%.

Based on the responses, a multiple linear regression was performed to investigate the effects of time, S/L ratio, and temperature on the leaching efficiency. In this analysis, the error was partitioned into components for lack of fit and pure error to test the adequacy of the model formally. Appendix Table 9 presents the overall model results for the REEs and for the other elements (Fe and B).

The lack-of-fit test was significant for Nd and Dy ($p < 0.05$), suggesting that the model did not capture all the variability of the data for these elements [34]. Although the small pure error estimated from the quadruplicate experiments may have contributed to the detection of statistically significant deviations [35, 36], this result represents a limitation of the models and should be considered when interpreting the predictions. Therefore, the Nd and Dy models should be regarded as empirical predictive models applicable within the investigated experimental domain rather than as general mechanistic models. For Pr, on the other hand, the lack of fit was not significant ($p > 0.05$), confirming the adequacy of the regression in this case. To further assess the overall quality of the models, residual analyses were performed.

Appendix Fig. 8(d–f) shows the residuals versus observation order, where only a slight trend can be noticed without systematic bias (Nd). In addition, Appendix Fig. 8(a–c) indicates that the residuals were randomly distributed with approximately constant variance, fulfilling the assumption of homoscedasticity [37]. The corresponding residual plots for the other elements are provided in Appendix Fig. 9. Considering these diagnostics together with the high determination coefficients ($R^2 = 0.9951$ [Nd] and 0.994 [Dy]) and the small residuals (<5%), the models were deemed suitable for describing the leaching behavior of REEs.

From the regression analysis, the statistically significant parameters ($p < 0.05$) were identified and are summarized in Appendix Table 10. Only the terms meeting the significance criterion were considered in the construction of the polynomial regression models, which are presented in Eqs. 13, 14, 15, 16, 17. Nonsignificant interaction and quadratic terms were excluded from the final models to avoid overparameterization and improve model interpretability. These factors were also highlighted in the Pareto charts for the REEs, shown in Appendix Fig. 10, which provides a visual representation of the relative importance of each effect. The corresponding Pareto plots for the other elements (Fe, and B) are also provided in Appendix Fig. 10.

$$\mathrm{Nd}(\%) = 97.32 + 7.77x_1 + 2.25x_2 + 28.25x_3 - 5.16x_1x_3 - 25.33x_3^2, \quad (13)$$

$$\mathrm{Pr}(\%) = 92.4 + 7.79x_1 + 2.25x_2 + 26.84x_3 - 1.89x_1x_2 - 4.57x_1x_3 - 23.76x_3^2, \quad (14)$$

$$\mathrm{Dy}(\%) = 95.18 + 8.24x_1 + 2.88x_2 + 30.61x_3 - 6.23x_1x_3 - 27.1x_3^2, \quad (15)$$

$$\mathrm{Fe}(\%) = 98.88 + 6.86x_1 + 32.38x_3 - 7.36x_1x_3 - 30.96x_3^2, \quad (16)$$

$$\mathrm{B}(\%) = 43.94 + 4.38x_1 + 16.73x_3 - 2.7x_1x_3 - 12.75x_3^2. \quad (17)$$

All studied factors (time, S/L ratio, and temperature) are statistically significant for Nd, Pr, and Dy. The temperature (x_3) exhibited the highest positive linear coefficient and the most negative quadratic coefficient. On the other hand, for Fe, B, and Co, only time and temperature significantly influence their leaching efficiency. No two-way (x_1x_2 or x_2x_3) or three-way interactions ($x_1x_2x_3$) were included in the regression model. This statistical behavior is consistent with the literature [38], which also reported that the individual impacts of temperature and time are among the most dominant factors, while their mutual interactions with other parameters exert a comparatively smaller influence on leaching performance.

The analysis of the response surface plots (Fig. 4) provided a visualization of the interactions between time, S/L ratio, and temperature, and their impact on the leaching efficiency. Based on the surface plots, temperature emerged as the most influential variable. The significant impact of this parameter explains the high leaching efficiencies achieved in this study, which contrast with results reported at room temperature, such as those by Romano et al. [30]. In their study, even with a higher acid concentration (3.0 mol L^{-1}), the REE leaching was limited to 64.6% due to a high

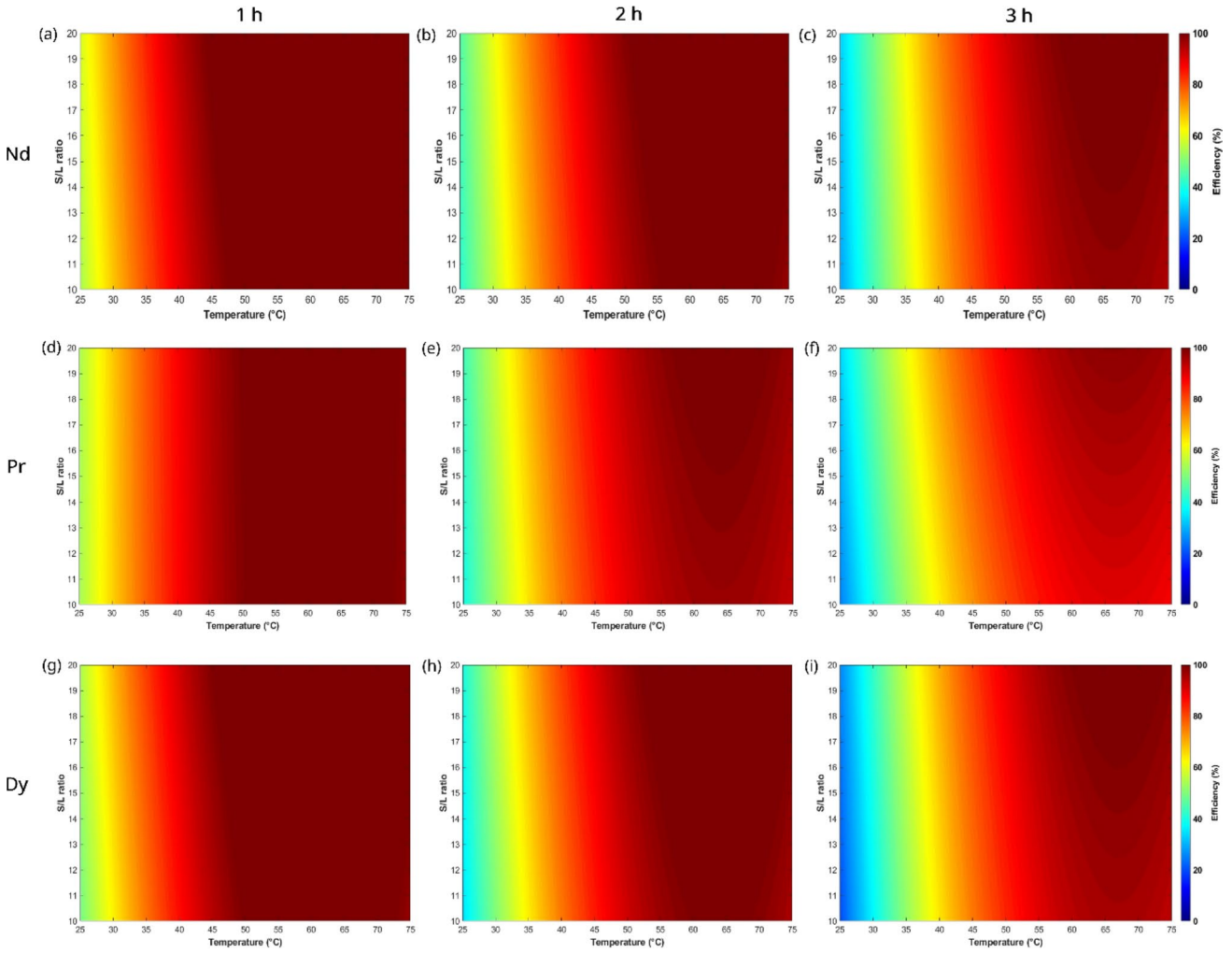

Fig. 4 Response surface plots for the leaching efficiency of Nd **a** 1 h, **b** 2 h, **c** 3 h; Pr **d** 1 h, **e** 2 h, **f** 3 h; Dy **g** 1 h, **h** 2 h, **i** 3 h

dependence on the S/L ratio, a limitation that is overcome in the present study by increasing the temperature.

A trade-off between time and temperature was observed. Reducing the reaction time from 3 to 2 h requires a temperature increase to maintain near-complete solubilization. The influence of time was more pronounced at lower temperatures. Furthermore, when operating at higher pulp densities (lower S/L ratios), longer reaction times were necessary to compensate for slower dissociation and reduced acid availability, respectively.

These results indicate that the optimal region is not restricted to a single condition but can be achieved through different combinations of time, temperature, and S/L ratio. The choice of operating conditions depends on the process objectives. If rapid leaching is required, higher temperatures are necessary to reach high leaching efficiencies in shorter reaction times. Conversely, when the goal is to minimize the S/L ratio, both temperature and time must be increased to compensate for the reduced acid availability.

Leaching efficiencies above 98% were achieved under several conditions, including 3 h, S/L of 1/13.3, 46 °C, and 1 h, S/L of 1/14.2, 62 °C. These conditions confirm the flexibility of the system and highlight the compensatory relationships among the studied variables, allowing the process to be adjusted according to the desired operational constraints.

Nevertheless, since the S/L ratio did not influence the leaching of Fe and B, (Eqs. 16, 17), their response surfaces exhibited a different pattern. The surface plots for all S/L ratio levels presented a similar shape for the elements (Fig. 5). As observed for the REEs, temperature was also the most influential variable in the leaching process.

The leaching efficiency of Fe followed a similar trend to that of the REEs, increasing from approximately 50% at 25 °C to nearly 100% at 46 °C. This behavior has been similarly reported in the literature for both mineral acids and organic acids [10, 28, 39]. The leaching of B also increased with temperature; however, its maximum leaching reached only 52%, even under the higher conditions studied (3 h, S/L of 1/20, 75 °C).

To validate the model, the condition of 2 h, S/L of 1/14.2, and 42 °C was randomly selected for experimental verification. After performing the tests in triplicate, the experimental results showed good agreement with the model predictions, as summarized in Appendix Table 11. The deviations between the predicted and experimental values were below 5.1% for most elements, confirming the reliability of the model.

Purification

For the purification stage, the liquor obtained at 75 °C, S/L ratio of 1/10 for 3 h was used, as this condition is within the optimal region identified by the DoE. The choice was based on the prior experimental reliability of this condition, ensuring high solubilization of the elements of interest. The resulting leachate contained 6.65 g L^{-1} of REEs (0.046 mol L^{-1}) and 14.88 g L^{-1} (0.18479 mol L^{-1}) of contaminants, as shown in Table 4, and exhibited a pH of 3.1 ± 0.1 and a redox potential of 200 mV.

Solvent Extraction

Effect of Extractant Concentration The influence of D2EHPA concentration (diluted in Isopar-L) on the extraction of (Nd, Pr, and Dy) was investigated within the range of 0.05 to 0.5 mol L^{-1}. To mitigate third-phase formation and optimize phase separation, TBP (3% v/v) was employed as a phase modifier [40]. The extraction percentages for the REEs and metallic impurities (Fe, Cu, Co, and B) are summarized in Table 5. Furthermore, the distribution coef-

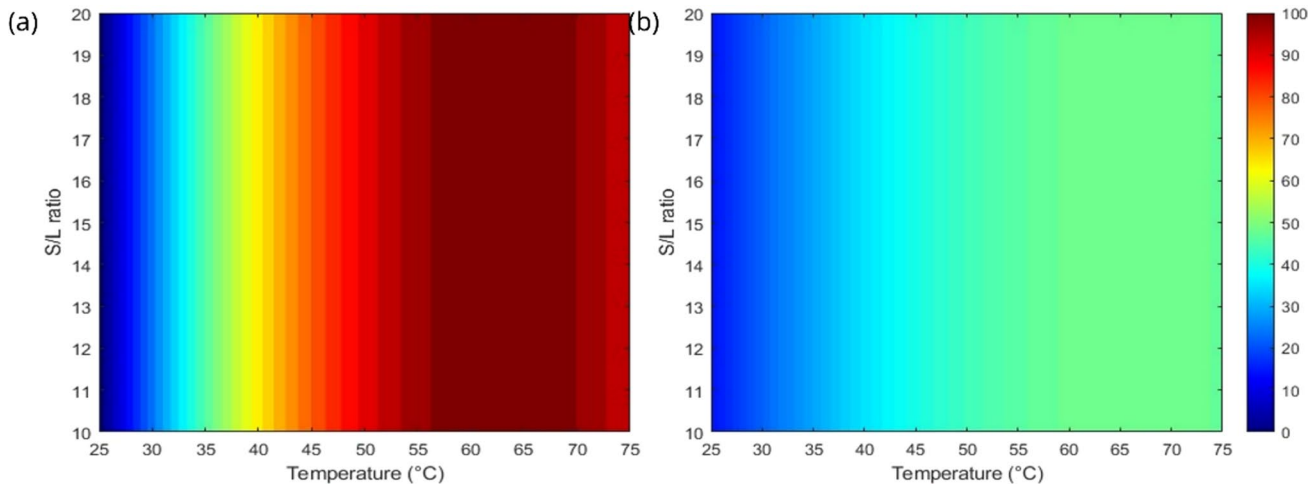

Fig. 5 Response surface plots of **a** Fe and **b** B

ficients and separation factors between the REEs and Fe are detailed in Appendix Table 5. The extraction mechanism using D2EHPA occurs predominantly through cationic ion exchange. In organic solutions containing aliphatic diluents, the extractant typically organizes into dimers, reacting with the metallic cation at the aqueous–organic interface [41]. The simplified stoichiometry of the extraction process can be expressed by Eq. 18, where M represents the metallic cation of valence n, $(HA)_2$ denotes the extractant dimer in the organic phase.

$$M^{n+}_{(aq)} + n(HA)_{2(org)} \leftrightarrow MA_n \cdot nHA_{n(org)} + nH^{+}_{(aq)}. \quad (18)$$

Table 5 demonstrates that increasing the D2EHPA concentration exerted a substantial effect on the recovery of Nd and Pr. Extraction efficiencies increased from 13.2% and 20.6% to 95.9% and 95.4%, respectively, as the concentration increased from 0.05 mol L^{-1} to 0.5 mol L^{-1}. This behavior is attributed to the shift in chemical equilibrium (Eq. 18) toward the formation of the organometallic complex, driven by the higher availability of the extractant's active sites. On the other hand, Dy extraction rates remained above 94.5% across all evaluated concentrations, demonstrating a distinct behavior compared with Nd and Pr. This high efficiency, even at low extractant concentrations, is attributed to the higher affinity of D2EHPA for heavy rare earth elements (HREEs) [42]. Due to the lanthanide contraction, Dy possesses a smaller ionic radius (1.027 Å) than Nd (1.109 Å) and Pr (1.126 Å), resulting in higher charge density and the formation of more stable complexes [43]. Additionally, the low initial Dy concentration (4.4 10^{-4} mol L^{-1}) in the feed solution ensures that, even at 0.05 mol L^{-1}, there is a stoichiometric excess of the extractant relative to this metal, allowing for high recovery rates regardless of the increase in D2EHPA concentration.

Concerning impurities, Fe exhibited a maximum extraction percentage of 30.1%. However, given the high initial concentration of this element in the feed solution, this percentage corresponds to a considerable mass co-extraction of approximately 4 g L^{-1}. Co and B exhibited low extraction rates, reaching maximum values of only 0.3% and 5.9%, respectively, at a concentration of 0.5 mol L^{-1}. This behavior is consistent with the selectivity of D2EHPA, which shows a higher affinity for trivalent cations (M^{3+}), such as REEs and Fe, over divalent cations like Co^{2+} or nonionic B species [44, 45]. In contrast, Cu displayed an inverse trend relative to the other elements: increasing the D2EHPA concentration from 0.05 to 0.5 mol L^{-1} led to a reduction in extraction from 86.1% to 70.3%. Although D2EHPA exhibits affinity for Cu at lower extractant concentrations, the increased loading of REEs (Nd and Pr) in the organic phase induced a crowding effect [46]. Due to the higher thermodynamic affinity of the extractant for trivalent lanthanide ions and the low initial Cu concentration (6.0 10^{-4} mol L^{-1}), the REEs preferentially

Table 4 Chemical composition of leach liquor

Element	Concentration	
	[g L^{-1}]	[mol L^{-1}]
Fe	14.37	2.6 10^{-1}
Nd	4.96	3.4 10^{-2}
Pr	1.62	1.2 10^{-2}
Dy	0.07	4.4 10^{-4}
B	0.22	2.0 10^{-2}
Co	0.23	3.8 10^{-3}
Cu	0.04	6.0 10^{-4}
Ni	0.02	3.9 10^{-4}

Table 5 Extraction percentages of REEs (Nd, Pr, Dy) and impurities (data represent the mean of experiments performed in triplicate: relative standard deviation < 0.5%)

		Nd	Pr	Dy	Fe	Cu	Co	B	pH
D2EHPA concentration (mol L^{-1})	0.5	95.9	95.4	99.2	30.1	70.3	0.3	5.9	2.8 ± 0.1
	0.3	76.1	80.7	96.6	17.1	75.7	1.2	0.1	2.8 ± 0.1
	0.1	41.6	36.1	98.4	18.8	78.1	1.0	0.6	2.9 ± 0.1
	0.05	13.2	20.6	94.5	1.0	86.1	1.2	2.3	2.9 ± 0.1
A/O ratio	1.0	94.3	95.4	99.2	30.1	70.3	0.3	5.9	2.8 ± 0.1
	1.5	85.0	87.4	97.8	24.6	41.6	ND	2.0	2.9 ± 0.1
	2.0	75.7	77.7	96.4	16.7	30.6	ND	2.5	2.9 ± 0.1
	2.5	62.5	65.6	94.2	11.0	25.6	ND	3.2	3.0 ± 0.1
Time (min)	5	95.9	96.9	100.0	23.1	61.3	ND	1.8	2.6 ± 0.1
	10	94.3	95.4	99.2	30.1	70.3	0.3	5.9	2.8 ± 0.1
	20	93.4	93.4	99.2	45.3	57.6	ND	1.3	2.8 ± 0.1
	30	93.5	93.5	99.1	45.1	64.9	0.4	2.3	2.7± 0.1
	60	90.0	92.2	98.7	52.8	53.3	0.1	1.8	2.8 ± 0.1

Table 6 Stripping efficiency of Nd, Pr, Dy, and impurities using HCl (0.1–0.7 mol L^{-1})*

Concentration (mol L^{-1})	Nd	Pr	Dy	Fe	Cu	Co	B
0.1	31.6	36.3	4.4	0.1	62.7	36.2	35.6
0.3	83.4	84.7	16.0	0.1	99.9	35.3	43.4
0.5	96.0	97.3	46.0	0.2	100	36.3	40.4
0.7	98.9	97.8	75.2	0.5	100	39.3	42.4

* Data are presented as the mean of triplicate measurements, with a relative standard deviation (RSD) < 0.3%

displace Cu from the D2EHPA active sites as the system approaches organic phase saturation.

A comparative analysis between the extraction percentages (Table 5) and the separation factors (Appendix Table 12) reveals a trade-off between recovery and selectivity. Although the 0.3 mol L^{-1} concentration yields the highest separation factors ($\beta_{Nd/Fe}$: 15.4 and $\beta_{Dy/Fe}$: 135.7), indicating a more selective process due to stoichiometric competition for D2EHPA active sites, the extraction efficiency for Nd and Pr decreases to approximately 76–80%. In contrast, the 0.5 mol L^{-1} concentration was selected as the optimal condition for the extraction stage, as it maximizes the recovery of the target REEs (> 95%). The observed decrease in separation factors at this concentration is a consequence of the higher extractant availability, which facilitates a more pronounced co-extraction of Fe (30.1%). However, from a process engineering perspective, the high recovery achieved at 0.5 mol L^{-1} justifies its selection, since the final selectivity regarding Fe can be further refined in subsequent scrubbing stages of the loaded organic phase.

Effect of A/O Ratio To optimize extractant consumption and evaluate the potential for metal enrichment in the organic phase, the effect of the A/O ratio was investigated, ranging from 1.0 to 2.5. For this study, the D2EHPA concentration was fixed at 0.5 mol L^{-1} (with 3% v/v TBP in Isopar-L), with a contact time of 10 min and an initial pH of 3.1. The extraction results are summarized in Table 5. A progressive decline in the extraction efficiency of Nd, Pr, Fe, and Cu was observed as the A/O ratio increased. For Nd and Pr, the extraction decreased by approximately 10% when shifting the ratio from 1.0 to 1.5, reaching a sharp reduction of 30% at a ratio of 2.5. This phenomenon is attributed to the decreased availability of extractant active sites relative to the metal mass in the aqueous phase. As the A/O ratio increases, the organic phase volume decreases proportionally, leading to premature saturation of the D2EHPA dimers and, consequently, reduced mass transfer [41, 47].

The lower extent of the reaction at higher A/O ratios is further supported by the equilibrium pH variation. Since the D2EHPA extraction mechanism is based on cation exchange (Eq. 18), the number of protons (H^+) released into the aqueous phase is directly proportional to the amount of metal extracted [48]. At an A/O ratio of 1.0, where extraction was highest, the pH dropped from 3.1 to 2.7. Conversely, at a ratio of 2.5, the final pH was 3.0, indicating lower H^+ liberation and confirming the reduced process efficiency under conditions of organic phase volume restriction.

Consistently with theoretical expectations, the decrease in extraction efficiency as the A/O ratio increases is accompanied by a systematic decline in D and $SF_{REE/Fe}$, as detailed in Appendix Table 12. The reduction in D values suggests that the organic phase approached its loading limit, thereby reducing the availability of free D2EHPA molecules for further metal extraction. Furthermore, the reduction in selectivity (D) indicates that, under high A/O ratio conditions, the competition for active sites becomes less favorable for separation, as the scarcity of available D2EHPA molecules reduces the discrimination between lanthanide ions and iron impurities.

Effect of Time To evaluate the kinetic behavior of the extraction process, contact time was investigated in the range of 5 to 30 min. The experimental conditions were maintained at a D2EHPA concentration of 0.5 mol L^{-1} (in Isopar-L with 3% v/v TBP), an A/O ratio of 1.0, and an initial pH of 3.1. The extraction percentages as a function of time are summarized in Table 5. The results indicate that the extraction kinetics for REEs are remarkably fast, reaching a near-equilibrium state within only 5 min. At this interval, extraction efficiencies reached 95.9% for Nd, 96.9% for Pr, and 100% for Dy. This rapid equilibrium is consistent with observations reported in the literature for organophosphorus extractants [32].

However, an increase in contact time led to a gradual decrease in the extraction of Nd, Pr, and Cu, whereas Fe extraction increased from 23.1% to 52.8%. This trend suggests that while the extraction of Fe is kinetically slower than that of the REEs [49], it possesses a high thermodynamic affinity for the D2EHPA active sites. Consequently, as Fe extraction progresses over time, a crowding effect occurs, where Fe^{3+} ions preferentially displace previously extracted elements with lower affinity, such as Cu and fractions of Nd and Pr. The impurities Co and B remained largely unaffected, maintaining extraction rates below 0.3% and 5.9%, respectively.

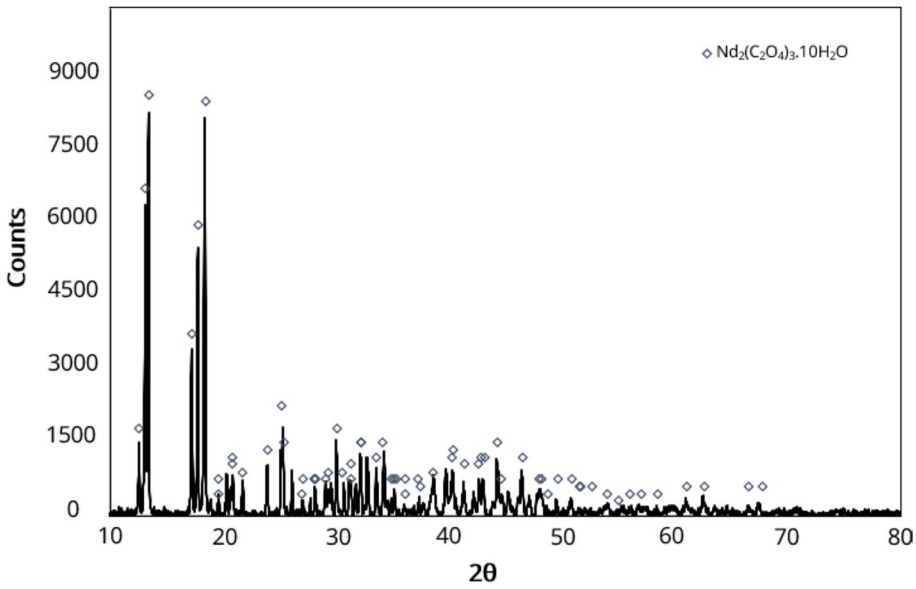

Fig. 6 XRD pattern of Nd oxalates resulting from the addition of H_2O_2 to citric acid liquor

Based on the combined studies of extractant concentration, A/O ratio, and reaction time, the optimized condition for REE recovery was identified as 0.5 mol L^{-1}, A/O 1.0, and 5 min. Nevertheless, to ensure system stability, data reproducibility, and to account for potential fluctuations in laboratory-scale mixing, a contact time of 10 min was selected for subsequent stages. It is worth noting that in a continuous industrial scale-up, where mass transfer equipment (e.g., mixer-settlers or centrifugal extractors) might offer different efficiencies, this residence time could be further reduced.

Following the extraction under the selected conditions, the resulting loaded organic phase contained Nd (4.961 g L^{-1}), Pr (1.565 g L^{-1}), Dy (0.071 g L^{-1}), Fe (4.347 g L^{-1}), Cu (0.018 g L^{-1}), Co (0.001 g L^{-1}), and B (0.011 g L^{-1}). The high concentration of impurities in the organic phase confirms the necessity of a dedicated back-extraction stage to remove them before the final recovery of REEs.

Stripping HCl was selected for the stripping stage, as it represents a well-established and industrially relevant approach for the separation and purification of REEs [50]. Stripping experiments were conducted with a 10-min contact time and an A/O ratio of 1.0, varying the HCl concentration from 0.1 to 0.7 mol L^{-1}. The stripping percentages are summarized in Table 6. The results demonstrate that the acidity of the aqueous phase is a critical factor in recovering the elements from the organic phase. By increasing the HCl concentration from 0.1 to 0.5 mol L^{-1}, stripping efficiencies of 96.0% for Nd and 97.3% for Pr were achieved, with minimal Fe co-stripping (0.2%). However, under these conditions, only 46.0% of Dy was recovered, highlighting the requirement for higher acidity to displace this element from the organometallic complex [51]. At an HCl concentration of 0.7 mol L^{-1}, the stripping efficiencies for Nd and Pr further increased, while Dy recovery reached 75.2%. Consistent with the findings in the extraction stage, the smaller ionic radius of Dy is the governing factor: its higher charge density results in a superior thermodynamic affinity for the organic phase (D2EHPA), making it more resistant to stripping than light lanthanides (Nd and Pr).

Table 6 also shows the stripping of impurities such as Cu, Co, and B. Despite high stripping efficiencies (up to 100%), their low initial concentrations in the organic phase ensure they do not significantly interfere with the final product's purity. After stripping with 0.7 mol L^{-1} HCl, the final aqueous solution concentrations were as follows: 4.906 g L^{-1} Nd; 1.531 g L^{-1} Pr; 0.053 g L^{-1} Dy; 0.022 g L^{-1} Fe; 0.018 g L^{-1} Cu; <0.001 g L^{-1} Co; and 0.005 g L^{-1} B. These results led to a rare earth product with a final purity of 99.3%.

Despite achieving a high final purity of 99.3%, the industrial implementation of the D2EHPA-based SX route presents significant technical hurdles that must be addressed. The most prominent operational challenge is the co-extraction of Fe. Due to the formation of highly stable thermodynamic complexes between Fe^{3+} and the D2EHPA dimers

Table 7 Overall REE recovery throughout the recycling routes based on the processing of 1 tonne of NdFeB magnets

Stage	Recovery (%)		
	Nd	Pr	Dy
After pretreatment	99.7	99.7	99.7
After leaching	99.7	98.7	96.7
SX route	93.0	92.0	72.0
Oxidative precipitation route	94.5	92.7	96.7

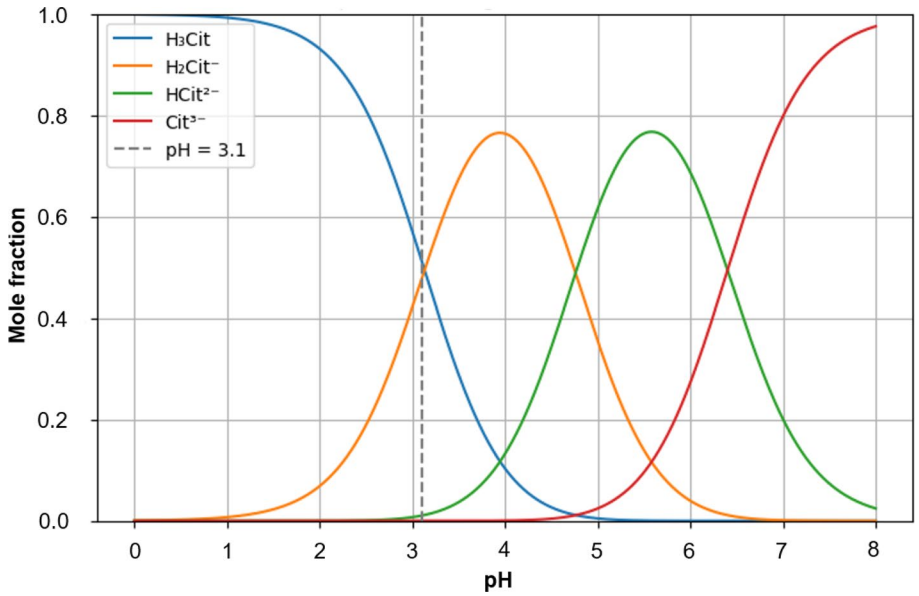

Fig. 7 Speciation diagram of citric acid showing the distribution of protonated and deprotonated species as a function of pH at 25 °C [64]

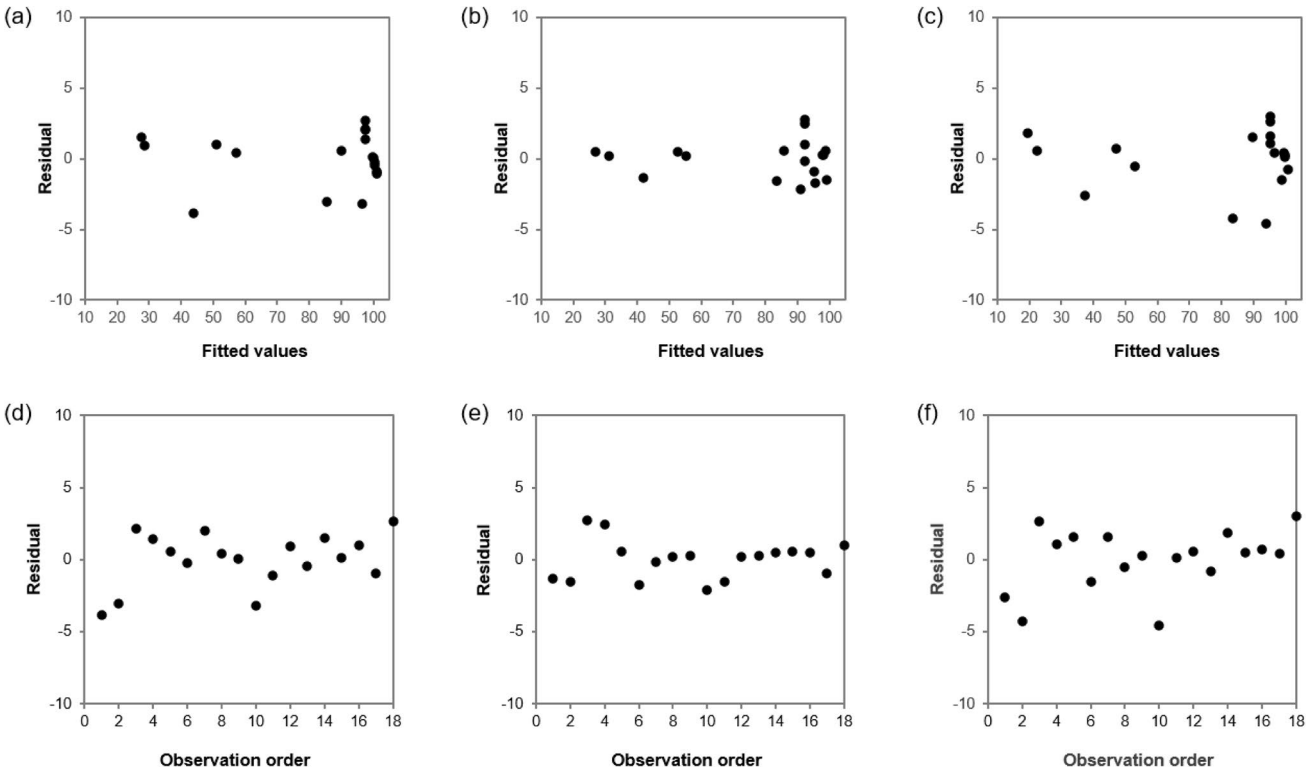

Fig. 8 Residual plots for the regression models: residuals versus observation order for **a** Nd, **b** Pr, and **c** Dy, and residuals versus fitted values for **d** Nd, **e** Pr, and **f** Dy

[52], removing this contaminant from the organic phase is notoriously difficult, a phenomenon widely recognized in the literature [53, 54]. Preliminary scrubbing trials indicated that effective iron removal requires high acidity levels (e.g., 5.0 mol L^{-1} HCl). However, such aggressive conditions pose a risk of hydrolytic degradation of the extractant over multiple cycles [55]. Given that D2EHPA is a high-value reagent designed for long-term regeneration and reuse, maintaining its chemical stability is a critical factor for the overall economic feasibility of the process.

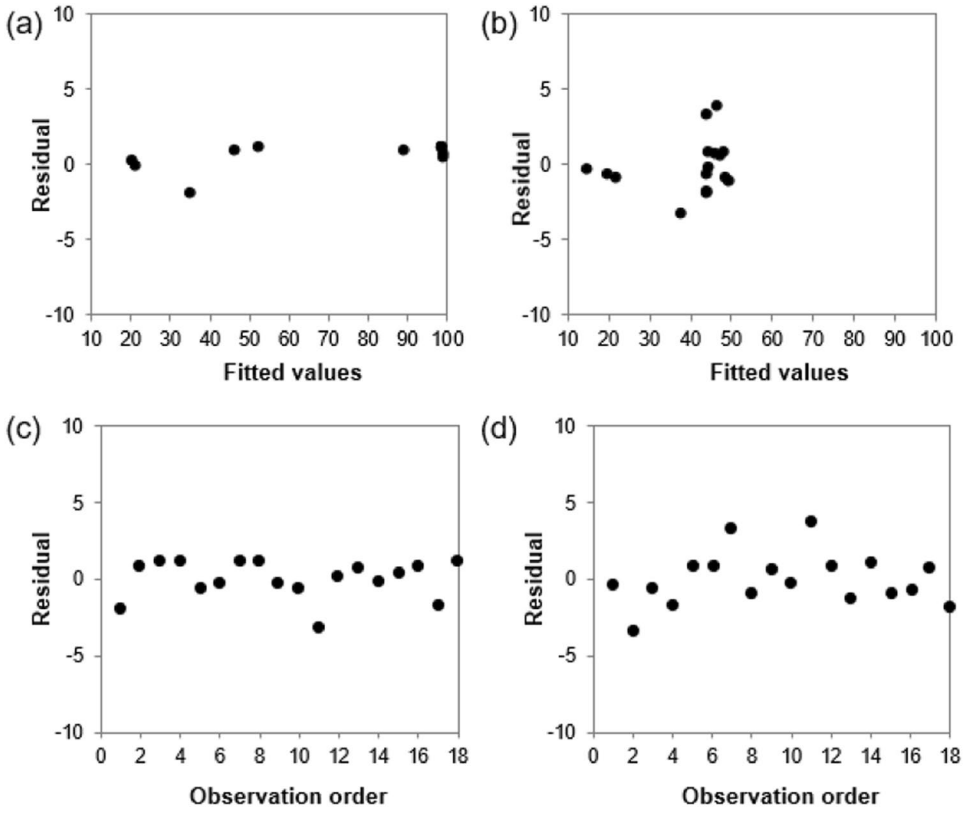

Fig. 9 Residual plots for the regression models: residuals versus observation order for **a** Fe and **b** B, and residuals versus fitted values for **c** Fe and **d** B

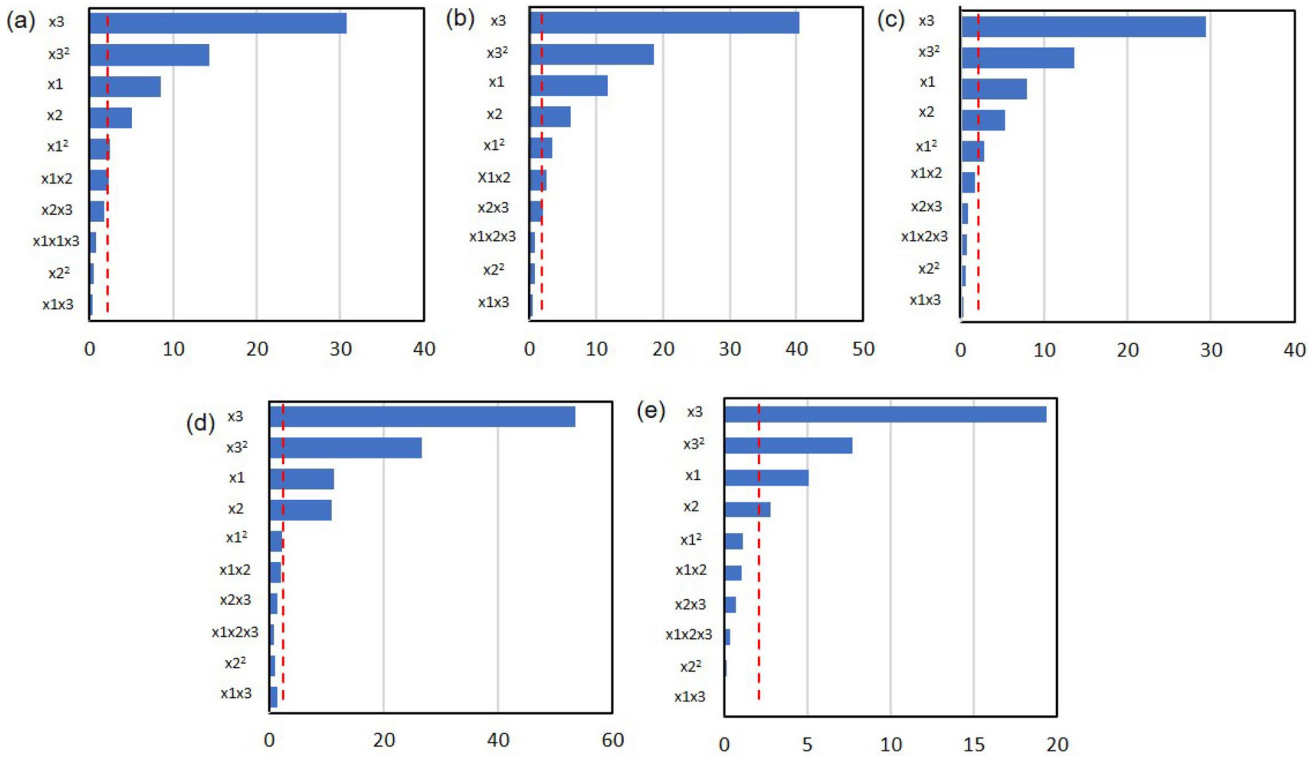

Fig. 10 Pareto charts of standardized effects for the regression models of **a** Nd, **b** Pr, **c** Dy, **d** Fe, and **e** B

Precipitation

The separation of the REEs present in the leach liquor was evaluated through selective precipitation using H_2O_2. The experiments resulted in high REE precipitation efficiencies: 94.8 ± 1.0% Nd, 93.0 ± 0.8% Pr, and 96.9 ± 1.0% Dy, along with 2.8% of Fe and 21.4% of Cu. This observation supports the hypothesis that H_2O_2 initiates an in situ Fenton-like reaction, catalyzed by the Fe ions inherent to the leachate solution [56]. As an advanced oxidation process (AOP), the Fenton mechanism, summarized in Eqs. 19–20, involves the reaction of H_2O_2 with Fe^{2+} to generate hydroxyl radicals ($\cdot OH$), highly reactive species capable of the nonselective oxidative degradation of organic compounds [57, 58].

$$Fe^{2+} + H_2O_2 \rightarrow Fe^{3+} + \cdot OH + OH^-, \tag{19}$$

$$Fe^{3+} + H_2O_2 \rightarrow Fe^{2+} + HO_2 \cdot + H^+, \tag{20}$$

$$\cdot OH + C_6H_8O_7 \rightarrow C_2H_2O_4 + CO_2 + H_2O + \text{subproducts}, \tag{21}$$

$$3C_2H_2O_4 + 2RE^{3+} + 10H_2O \leftrightarrow Re_2(C_2O_4)_3 \cdot 10H_2O_{(s)} + 6H^+. \tag{22}$$

This process facilitates the breakdown of larger citric acid molecules into shorter-chain organic acids, most notably oxalic acid [58]. This pathway proceeds through a series of multistep reactions involving sequential decarboxylation and the cleavage of carbon–carbon bonds [59]. In other words, it transforms the tricarboxylic acid structure into smaller dicarboxylic intermediates, as represented by the simplified overall reaction (Eq. 21). The formation of these oxalate ions subsequently drives the selective precipitation of REEs, as can be seen in Eq. 22 [60]. This proposed mechanism was confirmed by XRD analysis (Fig. 6), which identified the collected solid as a Nd oxalate phase ($Nd_2(C_2O_4)_3.10H_2O$).

Furthermore, the minimal Fe precipitation (~2.8%) confirms that iron remains predominantly in the aqueous phase. According to the literature, the oxidation state is critical for selectivity [61]. If Fe were present as Fe^{2+}, it would eventually precipitate in the form of Fe(II) oxalate once the saturation limit was reached. In contrast, as Fe is present as Fe^{+3}, oxalic acid deactivates the Fe cations through the formation of complexes in the coordination sphere, such as $[Fe(C_2O_4)]^+$, $[Fe(C_2O_4)_2]^-$, and $[Fe(C_2O_4)_3]^{3-}$ (Eqs. 23–25, Klemettinen et al., 2023). Consequently, Fe is left in the solution as a soluble complex.

$$C_2O^{2-}_{4(aq)} + Fe^{3+}_{(aq)} \leftrightarrow [Fe(C_2O_4)]^+_{(aq)}, \tag{23}$$

$$[Fe(C_2O_4)]^+_{(aq)} + C_2O^{2-}_{4(aq)} \leftrightarrow [Fe(C_2O_4)_2]^-, \tag{24}$$

$$[Fe(C_2O_4)_2]^- + C_2O^{2-}_{4(aq)} \leftrightarrow [Fe(C_2O_4)_3]^{3-}, \tag{25}$$

$$C_2O^{2-}_{4(aq)} + Cu^{2+}_{(aq)} \leftrightarrow CuC_2O_{4(s)}, \tag{26}$$

$$CuC_2O_{4(s)} + C_2O^{2-}_{4(aq)} \leftrightarrow Cu(C_2O_4)^{2-}_{2(aq)}. \tag{27}$$

Regarding the minor elements, although 21.4% of the Cu was co-precipitated, its impact on the final product purity is negligible, given that Cu represents only 0.18% (0.04 g L^{-1}) of the initial metal concentration. The partial precipitation of Cu can be explained by the equilibrium between the deposition of Cu oxalate (CuC_2O_4) and the formation of soluble oxalatocuprate(II) complexes (Eq. 26, 27, [61]). Based on the co-precipitation of B, Fe, and Cu, the purity of the recovered REE oxalate was determined to be 95.7%. Moreover, while the citric acid is converted into oxalate during the process, the remaining solution, rich in stable Fe(III) oxalate complexes, holds potential for valorization. Instead of being treated as waste, this effluent can serve as a precursor for lithium-iron-phosphate (LFP) battery materials or as a catalyst for AOPs, contributing to a more circular and sustainable recovery chain [62, 63].

Overall Process Evaluation and Mass Balance

To evaluate the overall performance of the proposed recovery routes, a process mass balance was established considering the treatment of 1 tonne of NdFeB magnets. The material flow was evaluated from pretreatment to the final purification stage, considering the recovery of the main REEs and the losses occurring throughout the process. The physical pretreatment steps resulted in a mass

loss of 0.32% (3.2 kg), corresponding to approximately 0.89 kg of REEs. After leaching under the optimized citric acid conditions (S/L ratio of 1/15, 75 °C, 3 h, and 1.5 mol L^{-1} citric acid), the recovery efficiencies reached 100% Nd, 99% Pr, and 97% Dy.

The purification strategies showed different recovery behaviors. The SX route using 0.5 mol L^{-1} D2EHPA followed by stripping with 0.7 mol L^{-1} HCl resulted in recoveries of 93% Nd, 92% Pr, and 72% Dy, achieving a final purity of 99.6%. The lower Dy recovery was associated with its stronger affinity for the D2EHPA phase, which limited its stripping efficiency. The oxidative precipitation route provided recoveries of 94.5% Nd, 92.7% Pr, and 96.7% Dy, demonstrating improved Dy retention compared with solvent extraction, although with lower product purity (95.7%). The overall REE recoveries obtained for each purification route are summarized in Table 7.

Conclusion

This study evaluated the leaching behavior of Nd, Pr, and Dy from NdFeB magnets using different organic acids. It demonstrated that citric acid is the most effective under the investigated conditions. After identifying the most suitable reagent, a DoE approach was applied to optimize the process. The optimization revealed that the leaching efficiency of citric acid can be achieved within a multidimensional operational window, rather than a single optimum. Depending on process priorities, high efficiencies may be obtained either by using elevated temperatures for rapid leaching or by increasing both time and temperature to compensate for lower S/L ratios.

Two purification strategies for REEs recovered from citric acid leachates were evaluated. SX using D2EHPA enabled high recovery of Nd and Pr, while Dy extraction was effective but its recovery was limited during the stripping stage, resulting in a REE-rich product containing 99.6% REEs. However, its application is associated with well-known limitations reported in the literature, particularly Fe co-extraction and the need for highly acidic scrubbing conditions. As an alternative, an oxidative precipitation route based on the in situ formation of oxalic acid via an Fe-catalyzed AOP yielded a mixed REE oxalate precipitate containing 95.7% REEs through a less complex purification approach. The choice between SX and oxidative precipitation, therefore, represents a trade-off between higher REE concentration and process simplicity, with both routes demonstrating potential for REE purification from citric acid leachates.

Appendix

Tables 8, 9, 10, 11, 12 and Figs. 7, 8, 9, 10..

Table 8 Experimental matrix of the face-centered cubic design with three factors at three levels

Experiment code	Order	Variables			Real variables		
		×1	×2	×3	Time (h)	S/L ratio	Temperature (°C)
1	14	−1	−1	−1	1	1/10	25
2	16	1	−1	−1	3	1/10	25
3	12	−1	1	−1	1	1/20	25
4	8	1	1	−1	3	1/20	25
5	5	−1	−1	1	1	1/10	75
6	15	1	−1	1	3	1/10	75
7	9	−1	1	1	1	1/20	75
8	13	1	1	1	3	1/20	75
9	3	0	0	0	2	1/15	50
10	18	0	0	0	2	1/15	50
11	7	0	0	0	2	1/15	50
12	4	0	0	0	2	1/15	50
13	2	−1	0	0	1	1/15	50
14	11	1	0	0	3	1/15	50
15	10	0	−1	0	2	1/10	50
16	17	0	1	0	2	1/20	50
17	1	0	0	−1	2	1/15	25
18	6	0	0	1	2	1/15	75

Table 9 Summary of regression and ANOVA of the fitted model results for the elements

Y	R^2	Source	Degrees of freedom	Sum of squares	Mean square	*F*-value	ρ-value
Nd		Regression	10	12,109.3	1210.9	143.6	0.0000004
		Residual	7	59.0	8.4	–	–
	0.9951	Lack of fit	4	58.2	14.6	53.0	0.004
		Pure error	3	0.8	0.3	–	–
		Total	17	12,168.3	–	–	–
Pr		Regression	10	10,629.0	1062.9	240.8	0.0000001
		Residual	7	30.9	4.4	–	–
	0.9971	Lack of fit	4	25.5	6.4	3.5	0.17
		Pure error	3	5.5	1.8	–	–
		Total	17	10,659.9	–	–	–
Dy		Regression	10	14,025.1	1402.5	129.8	0.0000001
		Residual	7	75.6	10.8	–	–
	0.9946	Lack of fit	4	73.3	18.3	23.3	0.01
		Pure error	3	2.4	0.8	–	–
		Total	17	14,100.8	–	–	–
Fe		Regression	10	15,752.3	1575.2	429.2	0.00000001
		Residual	7	25.7	3.7	–	–
	0.9984	Lack of fit	–	–	–	–	–
		Pure error	–		–	–	–
		Total	17	15,778.0	–	–	–
B		Regression	10	3833.8	383.4	51.5	0.00001
		Residual	7	52.1	7.4	–	–
	0.9866	Lack of fit	4	34.5	8.6	1.5	0.4
		Pure error	3	17.6	5.9	–	–
		Total	17	3885.9	–	–	–

Table 10 Statistically significant model terms identified by regression analysis

Element	Effect	Coefficient	Standard error	*t* statistic	*p*-value
Nd	Intercept	97.32	1.14	85.19	8.08E−12
	x_1	7.77	0.92	8.46	6.35E−05
	x_2	2.25	0.92	2.45	4.38E−02
	x_3	28.25	0.92	30.76	9.90E−09
	x_1x_3	−5.16	1.03	−5.03	1.51E−03
	x_3^2	−25.33	1.76	−14.36	1.89E−06
Pr	Intercept	92.40	0.83	111.78	1.21E−12
	x_1	7.79	0.66	11.72	7.44E−06
	x_2	2.25	0.66	3.39	1.16E−02
	x_3	26.84	0.66	40.39	1.49E−09
	x_1x_2	−1.89	0.74	−2.54	3.86E−02
	x_3^2	−23.76	1.28	−18.61	3.21E−07
Dy	Intercept	95.18	1.29	73.60	2.25E−11
	x_1	8.24	1.04	7.93	9.68E−05
	x_2	2.88	1.04	2.77	2.79E−02
	x_3	30.61	1.04	29.44	1.34E−08
	x_1x_3	−6.23	1.16	−5.36	1.05E−03
	x_3^2	−27.10	2.00	−13.57	2.77E−06
Fe	Intercept	98.88	0.75	131.19	3.94E−13
	x_1	6.86	0.61	11.32	9.38E−06
	x_2	32.38	0.61	53.45	2.10E−10
	x_1x_3	−7.36	0.68	−10.87	1.23E−05
	x_3^2	−30.96	1.16	−26.60	2.72E−08
B	Intercept	43.94	1.07	40.96	1.35E−09
	x_1	4.38	0.86	5.07	1.44E−03
	x_3	16.73	0.86	19.40	2.41E−07
	x_1x_3	−2.70	0.96	−2.80	2.64E−02
	x_3^2	−12.75	1.66	−7.70	1.16E−04

Table 11 Model validation through comparison of experimental and predicted leaching efficiencies

	Nd (%)	Pr (%)	Dy (%)	Fe (%)	B (%)
Experimental	88.0 ±0.6	81.9 ±0.1	85.1 ±1.0	94.0 ±0.2	37.3 ±0.1
Concentration	2462.5 ±200	783.0 ±22.0	35.0 ±0.5	7406.6 ±150	92.8 ±1.9
Model	85	80	81	93	37
Error	3.5	2.4	5.1	1.1	0.8

Table 12 REE–Fe separation behavior

		Distribution				Separation factor		
		Nd	Pr	Dy	Fe	Nd/Fe	Pr/Fe	Dy/Fe
D2EHPA concentration (mol L^{-1})	0.5	5.6	7.7	46.5	0.5	12.1	16.6	100.5
	0.3	3.2	4.2	28.0	0.2	15.4	20.2	135.7
	0.1	0.7	0.6	60.5	0.2	3.1	2.4	261.1
	0.05	0.2	0.3	17.1	0.0	15.0	25.5	1681.7
A/O ratio	1.0	5.7	6.9	44.9	0.3	17.4	21.2	137.8
	1.5	3.1	3.5	27.2	0.2	15.6	17.4	135.9
	2.0	1.7	1.9	16.2	0.1	13.4	15.4	130.4
	2.5	2.5	2.8	17.0	0.3	7.4	8.2	50.3
Time (min)	5	23.3	30.9	75.2	0.3	77.7	103.0	250.8
	10	5.7	6.9	44.9	0.3	17.4	21.2	137.8
	20	14.3	19.9	121.5	0.8	17.2	24.0	146.7
	30	14.4	19.7	114.2	0.8	17.6	24.1	139.2
	60	9.0	11.9	78.0	1.1	8.1	10.6	69.6

Acknowledgements The authors acknowledge the University of São Paulo for supporting this project and the São Paulo Research Foundation (FAPESP grants: 2024/05145-1, 2022/01159-2, and 2019/11866-5) for financial support. The information presented in this study is that of the authors and does not necessarily reflect the opinion of FAPESP. This work was also supported by Coordenação de Aperfeiçoamento de Pessoal de Nível Superior – Brasil (CAPES grant: 88887.507766/2020-00).

Funding The Article Processing Charge (APC) for the publication of this research was funded by the Coordenação de Aperfeiçoamento de Pessoal de Nível Superior - Brasil (CAPES) (ROR identifier: 00x0ma614).

Open Access This article is licensed under a Creative Commons Attribution 4.0 International License, which permits use, sharing, adaptation, distribution and reproduction in any medium or format, as long as you give appropriate credit to the original author(s) and the source, provide a link to the Creative Commons licence, and indicate if changes were made. The images or other third party material in this article are included in the article's Creative Commons licence, unless indicated otherwise in a credit line to the material. If material is not included in the article's Creative Commons licence and your intended use is not permitted by statutory regulation or exceeds the permitted use, you will need to obtain permission directly from the copyright holder. To view a copy of this licence, visit http://creativecommons.org/licenses/by/4.0/.

References

1. Kaya M (2024) An overview of NdFeB magnets recycling technologies. Curr Opin Green Sustain Chem 46:100884. https://doi.org/10.1016/j.cogsc.2024.100884
2. Agarwal C, Pandey AK (2023) Remediation and recycling of inorganic acids and their green alternatives for sustainable industrial chemical processes. Environ Sci Adv 2:1306–1339. https://doi.org/10.1039/D3VA00112A
3. Depraiter L, Goutte S (2023) The role and challenges of rare earths in the energy transition. Resour Pol 86:104137
4. Botelho Junior AB, Espinosa DCR, Vaughan J, Tenório JAS (2021) Recovery of scandium from various sources: a critical review of the state of the art and future prospects. Miner Eng 172:107148
5. Botelho Junior AB, Martins FP, Cezarino LO et al (2023) The sustainable development goals, urban mining, and the circular economy. Extr Ind Soc 16:101367. https://doi.org/10.1016/j.exis.2023.101367
6. Tesfaye F, Lindberg D, Hamuyuni J et al (2017) Improving urban mining practices for optimal recovery of resources from e-waste. Miner Eng 111:209–221. https://doi.org/10.1016/j.mineng.2017.06.018
7. Binnemans K, Jones PT, Blanpain B et al (2013) Recycling of rare earths: a critical review. J Clean Prod 51:1–22
8. Kumari A, Panda R, Jha MK et al (2015) Process development to recover rare earth metals from monazite mineral: a review. Miner Eng 79:102–115. https://doi.org/10.1016/j.mineng.2015.05.003
9. Uysal E, Al S, Emil-Kaya E et al (2022) Hydrometallurgical recycling of waste NdFeB magnets: design of experiment, optimisation of low concentrations of sulphuric acid leaching and process analysis. Can Metall Q. https://doi.org/10.1080/00084433.2022.2058152
10. Gergoric M (2018) Hydrometallurgical treatment of neodymium magnet waste. Chalmers Univesity of Technology
11. Petraglia FFN, Vinhal JT, Botelho Junior AB, Espinosa DCR (2024) Recycling of permanent magnets: a perspective for application of organic acids and ionic liquids towards eco-friendly process. J Environ Chem Eng 12:114389. https://doi.org/10.1016/j.jece.2024.114389
12. Reisdörfer G, Bertuol D, Tanabe EH (2019) Recovery of neodymium from the magnets of hard disk drives using organic acids. Miner Eng. https://doi.org/10.1016/j.mineng.2019.105938
13. Belfqueh S, Seron A, Chapron S et al (2023) Evaluating organic acids as alternative leaching reagents for rare earth elements recovery from NdFeB magnets. J Rare Earths 41:621–631. https://doi.org/10.1016/j.jre.2022.04.027
14. Zabiszak M, Nowak M, Hnatejko Z et al (2020) Thermodynamic and spectroscopic studies of the complexes formed in tartaric acid and lanthanide (III) ions binary systems. Molecules. https://doi.org/10.3390/molecules25051121

15. Vander Hoogerstraete T, Blanpain B, Van Gerven T, Binnemans K (2014) From NdFeB magnets towards the rare-earth oxides: a recycling process consuming only oxalic acid. RSC Adv 4:64099–64111. https://doi.org/10.1039/c4ra13787f
16. Petraglia FFN, Martins TAG, Hashimoto H et al (2025) Acetic acid leaching of rare earth elements from e-waste magnets: process optimization and kinetic evaluation. Waste Manag 205:115001. https://doi.org/10.1016/j.wasman.2025.115001
17. Banerjee R, Chakladar S, Mohanty A et al (2022) Review on the environment friendly leaching of rare earth elements from the secondary resources using organic acids. Geosyst Eng 25:95–115
18. Li F, Li X, Shi L et al (2024) Solvent extraction of scandium from leaching solution of red mud roasted with ammonium sulfate using D2EHPA/TBP. J Rare Earths 42:1943–1949. https://doi.org/10.1016/j.jre.2023.12.010
19. Mohammadi M, Forsberg K, Kloo L et al (2015) Separation of ND(III), DY(III) and Y(III) by solvent extraction using D2EHPA and EHEHPA. Hydrometallurgy 156:215–224. https://doi.org/10.1016/j.hydromet.2015.05.004
20. Zhang P, Liu Q, Huang J et al (2022) Phosphate conversion of electroplated Ni coatings on NdFeB magnets improving the anticorrosion property. J Alloys Compd. https://doi.org/10.1016/j.jallcom.2022.166206
21. Da Rocha Pereira B, Petraglia FFN, Espinosa DCR, Tenório JAS (2025) Hydrometallurgical innovations for recovery of rare earth elements from secondary sources: a comparative review. J Rare Earths. https://doi.org/10.1016/j.jre.2025.09.003
22. Tian Y, Liu Z, Zhang G (2019) Recovering REEs from NdFeB wastes with high purity and efficiency by leaching and selective precipitation process with modified agents. J Rare Earths 37:205–210. https://doi.org/10.1016/j.jre.2018.10.002
23. Martínez-Luévanos A, Rodríguez-Delgado MG, Uribe-Salas A et al (2011) Leaching kinetics of iron from low grade kaolin by oxalic acid solutions. Appl Clay Sci 51:473–477. https://doi.org/10.1016/j.clay.2011.01.011
24. Lee SO, Tran T, Park YY et al (2006) Study on the kinetics of iron oxide leaching by oxalic acid. Int J Miner Process 80:144–152. https://doi.org/10.1016/j.minpro.2006.03.012
25. Santawaja P, Kudo S, Mori A et al (2020) Sustainable iron-making using oxalic acid: the concept, a brief review of key reactions, and an experimental demonstration of the iron-making process. ACS Sustain Chem Eng 8:13292–13301. https://doi.org/10.1021/acssuschemeng.0c03593
26. Niskanen J, Lahtinen M, Perämäki S (2022) Acetic acid leaching of neodymium magnets and iron separation by simple oxidative precipitation. Clean Eng Technol. https://doi.org/10.1016/j.clet.2022.100544
27. Gergoric M, Ravaux C, Steenari BM et al (2018) Leaching and recovery of rare-earth elements from neodymium magnet waste using organic acids. Metals (Basel). https://doi.org/10.3390/met8090721
28. Romano P, Rahmati S, Adavodi R et al (2023) Leaching of rare earth elements from permanent magnet Swarf in citric acid: effects of acid concentration on extraction kinetics. Metals (Basel). https://doi.org/10.3390/met13111801
29. Behera SS, Parhi PK (2016) Leaching kinetics study of neodymium from the scrap magnet using acetic acid. Sep Purif Technol 160:59–66. https://doi.org/10.1016/j.seppur.2016.01.014
30. Belfqueh S, Chapron S, Giusti F et al (2024) Selective recovery of rare earth elements from acetic leachate of NdFeB magnet by solvent extraction. Sep Purif Technol 339:126701. https://doi.org/10.1016/j.seppur.2024.126701
31. Burdzy K, Aurich A, Hunger S et al (2022) Green citric acid in the sorption process of rare earth elements. Chem Eng J 437:135366. https://doi.org/10.1016/j.cej.2022.135366
32. Rouquette LMJ, Petranikova M, Vieceli N (2023) Complete and selective recovery of lithium from EV lithium-ion batteries: modeling and optimization using oxalic acid as a leaching agent. Sep Purif Technol 320:124143. https://doi.org/10.1016/j.seppur.2023.124143
33. Feng C, Li L, Sadeghpour A (2020) A comparison of residual diagnosis tools for diagnosing regression models for count data. BMC Med Res Methodol 20:175. https://doi.org/10.1186/s12874-020-01055-2
34. Li W, Cook D, Tanaka E, VanderPlas S (2024) A plot is worth a thousand tests: assessing residual diagnostics with the lineup protocol. J Comput Graph Stat 33:1497–1511. https://doi.org/10.1080/10618600.2024.2344612
35. Jarque CM, Bera AK (1980) Efficient tests for normality, homoscedasticity and serial independence of regression residuals. Econom Lett 6:255
36. Ray AR, Tripathy BC, Mishra S (2025) Investigation on process optimization and kinetics for leaching of rare earth elements from red mud using citric acid. Sci Rep. https://doi.org/10.1038/s41598-025-17134-7
37. Önal MAR, Borra CR, Guo M et al (2017) Hydrometallurgical recycling of NdFeB magnets: complete leaching, iron removal and electrolysis. J Rare Earths 35:574–584. https://doi.org/10.1016/S1002-0721(17)60950-5
38. Swami KR, Venkatesan KA, Antony MP (2019) Role of phase modifiers in controlling the third-phase formation during the solvent extraction of trivalent actinides. Solvent Extr Ion Exch 37:500–517. https://doi.org/10.1080/07366299.2019.1695560
39. Rodríguez Varela R, Chagnes A, Forsberg K (2025) Third-phase formation in rare earth element extraction with D2EHPA: key factors and impact on liquid membrane extraction performance. Membranes (Basel). https://doi.org/10.3390/membranes15070188
40. Rahmati S, Adavodi R, Romano P, Vegliò F (2025) Evaluation of the mechanisms of rare earth elements extraction from citrate solutions in the recycling of NdFeB magnets. Process Safety Environ Protect. https://doi.org/10.1016/j.psep.2025.106788
41. Hoshino M, Sanematsu K, Watanabe Y (2016) REE Mineralogy and Resources. pp 129–291
42. Junior CDSS, Nascimento M, Yokoyama L, Cunha OGCD (2012) Experimental design in solvent extraction: a study for divalent metals separation in D2EHPA/isoparaffin system. Engineering 04:816–825. https://doi.org/10.4236/eng.2012.411104
43. Rahmati S, Birloaga I, Romano P, Vegliò F (2024) Optimization of rare earth magnet recovery processes using oxalic acid in precipitation stripping: insights from experimental investigation and statistical analysis. Heliyon 10:e34811. https://doi.org/10.1016/j.heliyon.2024.e34811
44. Jeon JH, Yoon H-S, Kim C-J et al (2021) Environmentally sound technology development for processing of rare earth elements from waste permanent magnets synthetic leach solutions: recovery and separation perspectives. Sep Purif Technol 275:119225. https://doi.org/10.1016/j.seppur.2021.119225
45. Tunsu C, Menard Y, Eriksen DØ et al (2019) Recovery of critical materials from mine tailings: a comparative study of the solvent extraction of rare earths using acidic, solvating and mixed extractant systems. J Clean Prod 218:425–437. https://doi.org/10.1016/j.jclepro.2019.01.312
46. Essakhraoui M, Boukhair A, Bentiss F et al (2025) Advances in heavy metal extraction using organophosphorus compounds: a comprehensive review. Metals (Basel) 15:524. https://doi.org/10.3390/met15050524
47. Liu F, Porvali A, Halli P et al (2020) Comparison of different leaching media and their effect on REEs recovery from spent Nd-Fe-B magnets. JOM 72:806–815. https://doi.org/10.1007/s11837-019-03844-7

48. Merroune A, Ait Brahim J, Berrada M et al (2024) A comprehensive review on solvent extraction technologies of rare earth elements from different acidic media: current challenges and future perspectives. J Ind Eng Chem 139:1–17. https://doi.org/10.1016/j.jiec.2024.04.042
49. Alberts E, Dorfling C (2013) Stripping conditions to prevent the accumulation of rare earth elements and iron on the organic phase in the solvent extraction circuit at Skorpion Zinc. Miner Eng 40:48–55. https://doi.org/10.1016/j.mineng.2012.09.005
50. Jin Y, Ma Y, Weng Y et al (2014) Solvent extraction of Fe3+ from the hydrochloric acid route phosphoric acid by D2EHPA in kerosene. J Ind Eng Chem 20:3446–3452. https://doi.org/10.1016/j.jiec.2013.12.033
51. Zhou L, Zhang Y, Zhang L et al (2023) High-value recovery of the iron via solvent extraction from waste nickel-cadmium battery sulfuric acid leachate using saponified D2EHPA. Separations 10:251. https://doi.org/10.3390/separations10040251
52. Hu G, Wu Y, Chen D et al (2021) Selective removal of iron(III) from highly salted chloride acidic solutions by solvent extraction using di(2-ethylhexyl) phosphate. Front Chem Sci Eng 15:528–537. https://doi.org/10.1007/s11705-020-1955-4
53. Lupi C, Pilone D (2000) Reductive stripping in vacuum of Fe(III) from D2EHPA. Hydrometallurgy 57:201–207. https://doi.org/10.1016/S0304-386X(00)00112-2
54. Jiang Y, Ran J, Mao K et al (2022) Recent progress in Fenton/Fenton-like reactions for the removal of antibiotics in aqueous environments. Ecotoxicol Environ Saf 236:113464. https://doi.org/10.1016/j.ecoenv.2022.113464
55. Thomas N, Dionysiou DD, Pillai SC (2021) Heterogeneous Fenton catalysts: a review of recent advances. J Hazard Mater 404:124082. https://doi.org/10.1016/j.jhazmat.2020.124082
56. Ziembowicz S, Kida M (2022) Limitations and future directions of application of the Fenton-like process in micropollutants degradation in water and wastewater treatment: a critical review. Chemosphere 296:134041. https://doi.org/10.1016/j.chemosphere.2022.134041
57. Huston PL, Pignatello JJ (1999) Degradation of selected pesticide active ingredients and commercial formulations in water by the photo-assisted Fenton reaction. Water Res 33:1238–1246. https://doi.org/10.1016/S0043-1354(98)00330-3
58. Nawab A, Yang X, Honaker R (2022) Parametric study and speciation analysis of rare earth precipitation using oxalic acid in a chloride solution system. Miner Eng 176:107352. https://doi.org/10.1016/j.mineng.2021.107352
59. Pliego G, Zazo JA, Casas JA, Rodriguez JJ (2014) Fate of iron oxalates in aqueous solution: The role of temperature, iron species and dissolved oxygen. J Environ Chem Eng 2:2236–2241. https://doi.org/10.1016/j.jece.2014.09.013
60. Klemettinen A, Adamski Z, Chojnacka I et al (2023) Recovery of rare earth elements from the leaching solutions of spent NdFeB permanent magnets by selective precipitation of rare earth oxalates. Minerals. https://doi.org/10.3390/min13070846
61. Levanov AV, Isaikina OY, Lunin VV (2021) Solubility product and thermodynamic functions of copper (II) oxalate. Chem Eng Commun 208:1385–1394. https://doi.org/10.1080/00986445.2020.1780215
62. Ahile UJ, Wuana RA, Itodo AU et al (2021) Are iron chelates suitable to perform photo-Fenton at neutral pH for secondary effluent treatment? J Environ Manage 278:111566. https://doi.org/10.1016/j.jenvman.2020.111566
63. Hua Y, Zhang Z (2024) Ferrioxalate photolysis-assisted green recovery of valuable resources from spent lithium iron phosphate batteries. Waste Manag 183:199–208. https://doi.org/10.1016/j.wasman.2024.05.010
64. Martell AE, Smith RM (1982) Critical stability constants first supplement. Springer Science, Texas

Publisher's Note Springer Nature remains neutral with regard to jurisdictional claims in published maps and institutional affiliations.